Desalination 480 (2020) 114342

Contents lists available at ScienceDirect

Desalination

journal homepage: www.elsevier.com/locate/desal

Atomic scale manipulation of sublayer with functional TiO_2 nanofilm toward high-performance reverse osmosis membrane

Kiyoumars Zarshenas, Gaopeng Jiang, Jing Zhang, Mohd Altamash Jauhar, Zhongwei Chen*

Department of Chemical Engineering, University of Waterloo, 200 University Ave W, Waterloo, Ontario N2L 3G1, Canada

GRAPHICAL ABSTRACT

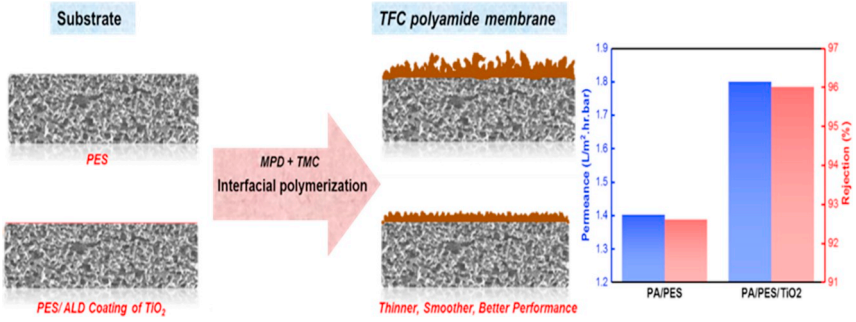

ARTICLE INFO

Keywords:
Thin-film composite membrane
Titanium oxide
Atomic layer deposition
Sublayer
Reverse osmosis

ABSTRACT

Recently, engineering the sublayer of polyamide thin film composite (PA-TFC) membrane by functional nanomaterials at nanoscale has been developed as an effective strategy to control interfacial polymerization reaction to fabricate high-performance reverse osmosis (RO) membrane. However, a reliable and practical manipulation technique is still needed to overcome the limitation of conventional sublayers. In this work, an approach of using atomic layer deposited (ALD) monomer-affinitive titanium dioxide (TiO_2) nanofilm to modify the sublayer of TFC was proposed to form a thin, smooth, and highly cross-linked PA selective top layer. The functional TiO_2 nanofilm increases the affinity between modified sublayer and amine monomer in favor of the efficient and subtle tuning of the adsorption and diffusion of amine monomer during the interfacial polymerization process. The obtained TFC membrane with optimal ALD TiO_2 coverage demonstrates well-improved RO performance in terms of high permeance of 1.8 $L.m^{-2}.h^{-1}.bar^{-1}$ and high salt rejection rate of 96.1% in a dead-end process. This work reveals that coating functional nanomaterials by ALD is a practical manipulation technique toward the controllable fabrication of promising TFC membrane and the optimization of sublayer materials.

1. Introduction

Water scarcity, a growing global concern, has led to a broad interest in membrane desalination technology [1]. Reverse osmosis (RO) is one of the dominant and efficient methods for generating pure water from saline water and other sources of wastewater [1–3]. The cutting edge choice for RO desalination is the polyamide thin film composite (PA-TFC) membranes [4,5]. In general, PA-TFC membranes are fabricated on porous polymeric support by the in-situ polycondensation of two reactive monomers, namely polyamine and polyacyl chloride, at the interface of two mutually immiscible solvents [6,7]. Among several synthesis factors of interfacial polymerization (IP) which impact the

* Corresponding author.
E-mail address: zhwchen@uwaterloo.ca (Z. Chen).

https://doi.org/10.1016/j.desal.2020.114342
Received 13 October 2019; Received in revised form 17 January 2020; Accepted 18 January 2020
Available online 07 February 2020

separation performance and the physicochemical properties of TFC membranes, the sublayer properties play one of the most significant roles [8,9]. It includes structural properties (pore size distribution, porosity, pore density, and roughness) and chemical properties (hydrophilicity-hydrophobicity and the affinity/reactivity with amine or acyl chloride monomers) [10–17]. Conventional sublayers for TFC membrane consist of polymeric ultrafiltration (UF)/microfiltration (MF) membranes, which generally have poor surface wettability, rough surface, and low porosity [18]. An effective strategy to overcome these limitations is to modify a sublayer by functional nanomaterials to mediate the adsorption and diffusion rate of the amine monomer, the uniformity of both monomer distribution, the IP reaction rate [8,18,19]. The innate properties of functional nanomaterials such as hydrophilicity, antifouling, affinity interactive, photocatalytic and others, equip the membrane with desirable properties [20].

Recently, several different manipulation methods have been proposed to modify the sublayer by functional nanomaterials. One strategy is to add inorganic and hydrophilic additive to the sublayer [21–23]. For instance, Wang et al. [21] fabricated the high performance RO membrane with thin and compact PA selective layer by incorporating tannic acid into the support layer, which enhanced the hydrophilicity of the support layer, and varied the absorption/diffusion behavior of the amine and the formation of the nascent film. However, the homogenous dispersion of additive in the sublayers is challenging [8] Alternatively, the application of a specific interlayer [24–33] or sacrificing layer [34,35] was reported via vacuum filtration or interfacial self-assembly. For example, Livingston et al. [34] utilized a hydrophilic and uniform cadmium hydroxide nanostrand interlayer, which works as a container for the aqueous solution of the amine monomer, to regulate and optimize the formation of the skin layer with exceptional permeability. Applying sacrificing layer not only results in poor integrity between polyamide top layer and sublayer, but also makes the TFC membrane preparation procedure complicated due to additional removal steps of sacrificing layer after IP. Also, using these techniques would result in a relatively small area membrane. Therefore, the design of desirable sublayer by functional nanomaterials needs a reliable and practical manipulation strategy for controllable IP reaction at large area. Atomic layer deposition (ALD) as a versatile technology with outstanding properties [36] and feasible up-scaling [37–39] in membrane preparation [39–43], able to coat thin film of various high quality materials (inorganic metal oxides, metals, etc.) on substrates at the nanoscale with accurate thickness control, great uniform coverage and outstanding conformality.

Here, in this study, for the first time, a novel strategy of atomic scale surface modification by functional nanomaterial was proposed to tune the physicochemical properties of the sublayer to design high-performance PA-TFC membrane. Atomic layer deposition (ALD) was used to coat an ultrathin layer of monomer-affinitive TiO_2 on porous polyethersulfone (PES) sublayer. Such a novel and rational approach adapts the following advantageous features: (i) ALD offers a great uniform and size control [44] coating of TiO_2 which controllably boosts uniformity and smoothness of the sublayer at nanoscale. (ii) The ALD coated TiO_2 layer with outstanding hydrophilicity, porosity [31,45], and stability [46–49], entirely covers the surface of the PES and firmly integrate with the PES layer [50]. Moreover, TiO_2 nanofilm's functionality of tuning up the affinity of sublayer to the amine monomer further mediates absorption/diffusion behavior of the amine monomer in the interfacial polymerization process. (iii) The optimal ALD TiO_2 coverage leads to a thin, smooth, and highly cross-linked PA selective top layer. As a result, improved RO performance was obtained for the optimal TFC in a dead-end process in terms of high permeance of 1.8 $L.m^{-2}.h^{-1}.bar^{-1}$ and high salt rejection rate of 96.1%. Atomic scale manipulation of sublayer by ALD opens a new path toward controlling IP and preparing high-performance RO membranes.

2. Experimental

2.1. Materials

As reacting monomers, trimesoyl chloride (TMC) 98% and *m*-phenylenediamine (MPD) 99% were provided from Sigma-Aldrich. Anhydrous Hexane (≥99%) as the organic solvent, triethylamine (TEA), sodium dodecyl sulfate (SDS), dimethyl sulfoxide (DMSO), and camphorsulfonic acid (CSA) were used as the additives and supplied from Sigma-Aldrich. PES sublayer (average pore size of 0.1 μm) was purchased from Sterlitech Co. (WA, USA). The purchased materials and membranes were used without further modification.

2.2. Deposition of TiO_2 film on PES sublayer and ALD condition

An ultrathin film of TiO_2 was directly coated on the PES membrane at 95 °C in an ALD system (Thermal Gemstar 6XT, Arradiance, LLC, USA). Firstly, using deionized water (DDI water), PES membranes were washed then dried for 8 h at 70 °C. Afterwards, the membrane samples were placed in the holder of an ALD system, preheated at 95 °C for 30 min under vacuum (~ 30 mTorr). Each ALD cycle consisted of (1) insert a first precursor (a pulse of 700 mSec of titanium tetraisopropoxide (TTIP, $Ti(OCH(CH_3)_2)_4$) heated at 60 °C for a determined exposure time to allow the TTIP to react with the membrane surface), (2) Purging the chamber with the carrier gas (pure N_2) with a flow rate of 200 sccm to remove a remaining unreacted precursor or any by-products, (3) insert the water into the process as an oxygen reactant source (a pulse time of 22 mSec of H_2O) to form the TiO_2, and (4) again N_2 purging to remove excess water and by-products from the chamber. By repeating this cycle, TiO_2 film with the accurate thickness can be deposited on the sublayer. In this study, different ALD cycles (0, 10, 50, 100, 200) were performed on PES sublayer and the obtained modified sublayers for further IP were denoted as ALD-x-TiO_2@PES, where x means the number of ALD cycles.

2.3. Polyamide thin film composite (PA-TFC) membrane preparation

The PA-TFC membranes were synthesized by modified IP procedure (filtration method) via a vacuum filtration lab-scale setup [51]. In this filtration technique firstly, a 2 w/v% of MPD solution (25 mL) containing 0.1 w/v% SDS, 1 w/v% CSA, 1 w/v% TEA and 1 w/v% DMSO was poured onto the support layer. After 10 min of contact time, the MPD solution was filtered through the support layer by vacuum pressure (applied vacuum of 0.1 bar below atmosphere) to distribute MPD evenly on the surface of the support. Then, the excess solution was air-dried until no observed droplets. Support membrane was contacted with the organic phase (0.15 w/v% of TMC in hexane) (25 mL) which was removed by pouring out from the top of filtration flask, after 30 s. Then, the membrane surface was washed by n-hexane (100 mL) to eliminate unreacted monomers. The resulting membranes were cured at 60 °C for 4 min. Lastly, using DDI water, the fabricated TFC membranes were washed to remove the remaining reactants and then placed in lightproof DDI water container for performance evaluation and characterization. The obtained TFC membranes on different ALD-x-TiO_2@PES sublayers are denoted as PA-TFC-x, where x stands for the number of ALD cycles that was applied for TiO_2 nanoparticle coating.

2.4. Physicochemical characterization

The surface and cross-sectional morphologies of the membranes were detected by high resolution scanning electron microscopy (SEM, LEO FESEM 1530) with an accelerating voltage of 10 KV. For the cross-sectional analysis, membranes were broken in liquid nitrogen, and gold sputtering was used for all membrane samples before Field Emission Scanning electron microscopy (FE-SEM) detection. Energy dispersive X-ray spectroscopy (EDS) attached to a FE-SEM was applied to measure

elemental composition specially the total amount of Ti atoms on the modified PES support membrane. The distribution of pores of the support layer was assessed by studying FE-SEM images of the modified PES membrane utilizing the ImageJ software. To study the surface topology of the membranes, Atomic Force Microscopy (AFM) (Bruker Innova AFM, USA) was utilized in tapping-mode. At least three times each membrane sample was scanned over a surface area of 10 μm by 10 μm, then the obtained AFM data was processed using Gwyddion analysis software, eliminating the noise and calculating the root mean square (R_q) and the average (R_a) roughness values.

The elemental compositions (C, O, and N) of the TFC PA membrane surfaces were studied via an X-ray photoelectron spectroscopy (Thermal Scientific K-Alpha XPS spectrometer). The cross-linking degree can be calculated by XPS spectra. The based on the chemical formula of fully linear ($C_{15}H_{10}O_4N_2$) and fully cross-linked ($C_{18}H_{12}N_3O_3$) polyamide, the theoretical O/N ratio can be shown by:

$$\frac{O}{N} = \frac{3m + 4n}{3m + 2n} \tag{1}$$

and cross-linking degree (%) of the whole PA selective layer (not only the incipient layer) can be calculated by:

$$D = \frac{m}{m + n} \times 100 \tag{2}$$

where n and m are the linear and cross-linked proportion of the PA selective layer, respectively, and XPS analysis results are used to determine the values of n and m [52,53].

The surface hydrophilicity of support layer was evaluated through contact angle measurements by means of an optical instrument (OCA20, Data Physics, Germany) at room temperature. Using a motorized micro syringe, a preset 5 μL droplet of DDI water was formed at the tip of a steel needle (20 gauge, 0.603 mm in diameter) placed on the surface of membrane and images of this drop were captured by a CCD camera. Image acquisition and determination of contact angle by automated drop shape analysis (ADSA) were implemented utilizing the VCA 2500 XE equipment and software (AST Products, Billerica, MA). For each sample, the static contact angle was assessed at 5 various locations to minimize the experimental error.

Membrane partition coefficient of MPD (K_m) was measured to determine the affinity of MPD to sublayer membrane [54]. Also, the solution uptake (SU) was used to determine the amount of solution taken up by the membrane sublayer [55]. The sublayer membranes were cut into the square pieces 1.5″ in length. The pieces were then immersed in 50 mL of aqueous 2 wt% MPD solution for 10 min. K_m and SU can be calculated by:

$$K_m = \frac{C_{MPD}^{membrane}}{C_{MPD}^{H_2O}} = \frac{\frac{m_2 - m_0}{m_1 - m_0}}{C_{MPD}^{H_2O}} \tag{3}$$

$$\mathrm{SU}(\%) = \frac{m_1 - m_0}{m_0} \times 100 \tag{4}$$

where m_1 depicts the sublayer weight saturated with MPD solution, m_0 and m_2 depicts the weight of dry sublayer before and after immersing in the MPD solution, respectively. Based on the Beer-Lambert law, the concentration of MPD in the water phase was measured at a certain time interval by an Ultraviolet–visible spectrophotometer (GENESYS 10S UV–Vis Thermo Fisher Scientific) using its absorbance at a wavelength of 292 nm, therefore, the MPD concentration ($C_{MPD}^{H_2O}$) of the solution could be calculated after immersion of each sublayer.

2.5. Membrane performance test

Dead-end filtration system (Sterlitech HP4750 Stirred Cell) were used to investigate the rejection and pure water permeability of the prepared membranes. In order to pressurize the membrane cell, a nitrogen gas cylinder attached with the pressure regulator was linked to the top of container. The prepared TFC membrane was cut into the determined shape (effective area was 14.6 cm^2) and placed in the membrane cell. The solution volume was 250 ml. The membranes were initially compacted at a constant temperature of 25 °C and a trans-membrane pressure of 20 bar with DI water for approximately 1 h. After the compaction, the initial water flux was measured for 10 min. Permeate was gathered via graduated cylinder for a period of time till steady condition. The pure water permeability (PWP) ($L.m^{-2}.h^{-1}.bar^{-1}$) was calculated by:

$$PWP = \frac{\Delta V}{\Delta t} \frac{1}{A_m \Delta P} \tag{5}$$

where ΔP (bar) is the applied trans-membrane pressure, A_m(m^2) is the effective area of the membrane testing cell, Δt(h) is the elapsed time period of sample collection, and ΔV (L) is the volume of collected permeate. In the salt rejection test, a brackish water (2 g/L NaCl) was utilized as the feed solution. A bench conductivity meter (Hanna HI 8733) was utilized to measure the conductivity in the permeate (σ_p) and feed (σ_f). At least 40 ml solution was collected each time for the measurement. The membrane salt rejection calculation was performed by the conductivity ratio between the permeate solution (σ_p) to the feed solution (σ_f) [56].

$$R\ (\%) = \left(1 - \frac{\sigma_p}{\sigma_f}\right) \times 100 \tag{6}$$

For each TFC membrane, at least three similar membranes were prepared with the same procedure and were analysed to calculate the average salt rejection, pure water permeability, and the standard deviation was indicated by the error bar.

3. Results and discussion

3.1. ALD coating and the properties of ALD-x-TiO_2@PES sublayers

As shown in Fig. 1, fabrication of TFC polyamide membranes consist of the following two steps: (a) Deposition of TiO_2 layer on the PES sublayer (b) Polyamide interfacial polymerization on the modified sublayer.

TiO_2 ALD nucleation growth on the PES that lacks reactive groups like hydroxyl, can be described by different mechanism [57–59] in comparison to the normal ALD growth. The PES sublayer, which has a porous surface, and TTIP are nonpolar. Therefore, TTIP is anticipated to have a decent solubility in the PES, and TTIP can adsorb to the surface of the PES and afterwards diffuse to the PES sublayer's near-surface area. During the ALD reaction, the arriving H_2O will react effectively with TTIP molecules at or near the surface of the PES sublayer and TiO_2 clusters will be formed. After the nucleation of TiO_2, the reaction for the cycle of TiO_2 ALD can be defined as below [60,61]:

$[Ti(OH)_x]^* + Ti(OCH(CH_3)_2)_4 \rightarrow [TiO_xTi(OCH(CH_3)_2)_{4-x}]^* + xCH(CH_3)_2OH$	(1st half reaction)
$[TiO_xTi(OCH(CH_3)_2)_{4-x}]^* + 2H_2O \rightarrow TiO_2 + [Ti(OH)_x]^* + (4 - x)CH(CH_3)_2OH$	(2nd half reaction)
$Ti(OCH(CH_3)_2)_4 + 2\ H_2O \rightarrow TiO_2 + 4CH(CH_3)_2OH$	(Total reaction)

By repeating the ALD cycle, an ultrathin layer of TiO_2 with the amorphous structure was obtained in the low temperature [62,63]. Fig. 2K, which is proportional to the Ti EDS intensity [42], and Fig. S1, which is EDS mapping of Ti element, can confirm that the amount of TiO_2 on the PES support layer increases when the ALD cycle is increased. Also, it indicates that TiO_2 deposition successfully coated on

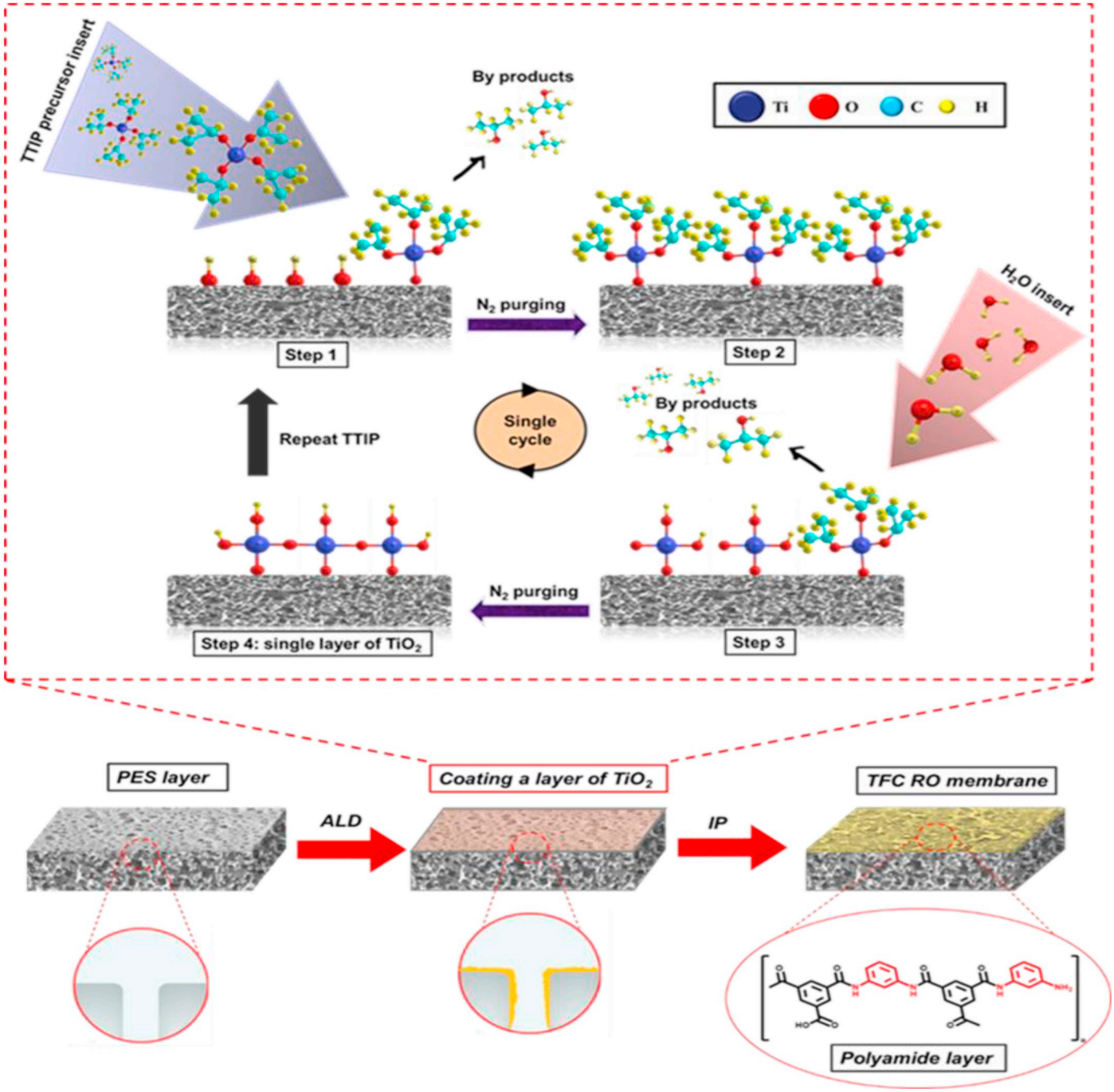

Fig. 1. Schematic representation of TFC RO membrane with modified PES support layer and one ALD cycle of TiO_2 deposition on the PES sublayer.

the PES support layer surface and pore walls.

Fig. 2 (A-J) shows the SEM and AFM images of ALD-x-TiO_2@PES membranes. The FE-SEM images of ALD-x-TiO_2@PES (Fig. 2(B-E)) indicate almost no changes in the surface morphology compared to the pristine membrane (Fig. 2A) which may be due to conformal and uniform deposition of modified layers. Based on the growth rate of TiO_2 reported by literature in the same experimental ALD condition [60], the growth rate of TiO_2 is reported around 0.04 nm per cycle. Therefore, for ALD 200-TiO_2@PES the nominal thickness of TiO_2 is considered around 8 nm and it can be estimated that the pore size reduction is around 5 to 10 nm. Thus, the effect of these range of ALD cycle on the morphology and pore size of the sublayer can be considered negligible. According to the AFM images in Fig. 2(G-J), the homogenous deposition of TiO_2 nanoparticles clearly reduced the surface roughness of sublayers, declining from 53 nm in average for pristine PES membrane to 37 nm in average for ALD-200-TiO_2@PES (Fig. 2J).

Such smooth surface of sublayer is favorable for the following IP of the PA top layer. The surface hydrophilicity was determined by the water contact angles (WCAs) measurement. WCA continuously decreased as the number of ALD cycles increased (Fig. 2M). The contact angle decreased from 62 to 41 for PES membranes with 10 ALD cycles. This result showed that PES surfaces were not fully covered by TiO_2 during this stage and discrete coating of TiO_2 is on the surface of PES layer. At 200 ALD cycles, the contact angle reduced considerably to 11, because of the formation of a continuous film of TiO_2. These results suggest that the ALD-coated TiO_2 nanoparticles considerably enhance the surface wettability of the PES sublayer, which enables the amine solution to homogeneously spread on the coated support surface. The

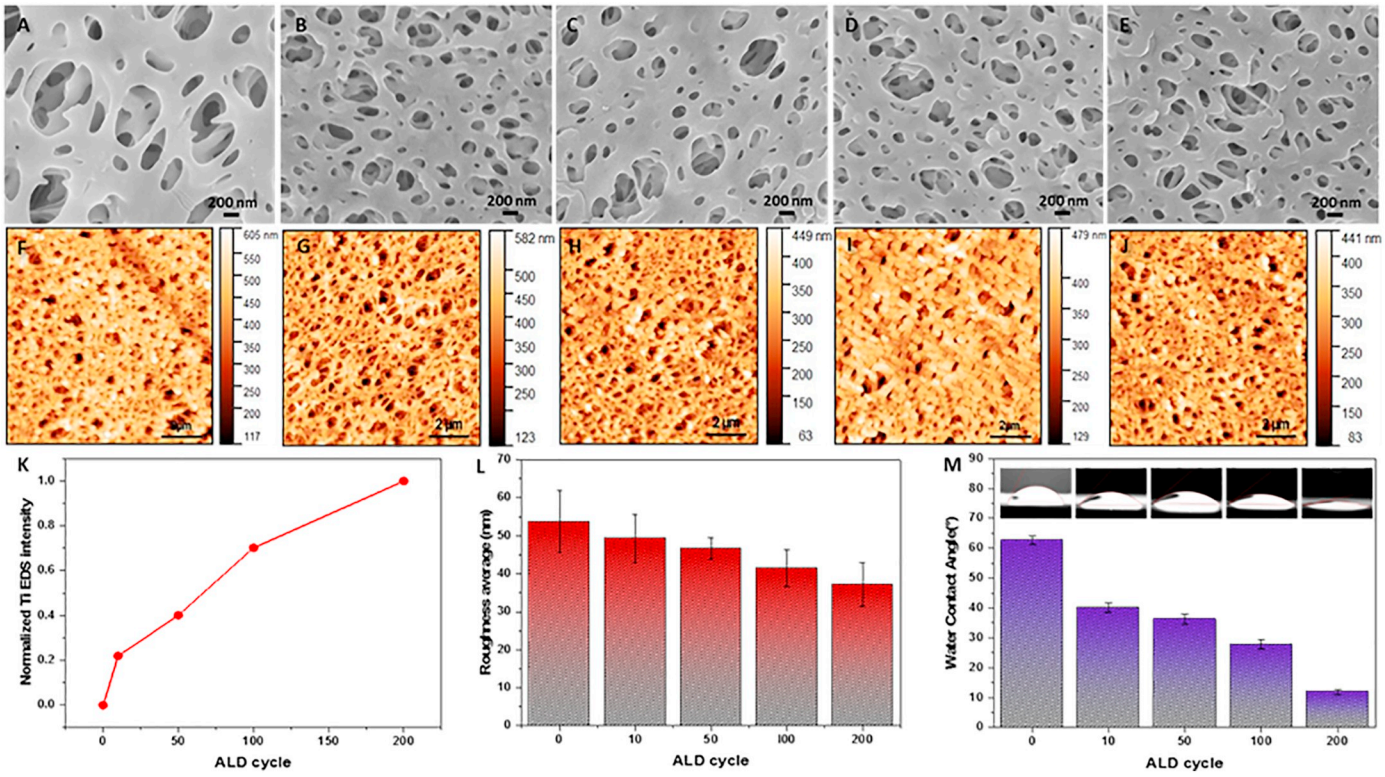

Fig. 2. Properties of PES sublayer with different TiO_2 ALD cycles: (A to E) SEM surface images and AFM images (A, F) pristine PES, (B, G) ALD 10-TiO_2@PES, (C, H) ALD 50-TiO_2@PES, (D, I) ALD 100-TiO_2@PES, (E, J) ALD 200-TiO_2@PES, (K) Normalized Ti Peak area in SEM-EDS spectra, (L) Ra surface roughness, and (M) water contact angle.

tunable wettability toward high hydrophilicity for PES sublayer via ALD coating of TiO_2 nanoparticles will further favor in the formation of the PA selective layer [21,29].

Solution uptake is measured to understand the adsorption and diffusion behavior of MPD. The solution uptake increases from 3.114% for the pristine PES sublayer to 4.781% for the ALD-200-TiO_2@PES. According to the results, PES-TiO_2 membranes absorb more MPD than pure PES membranes, which enhances the concentration of MPD in the membrane and, subsequently, increases the amount of MPD in the reaction zone for interfacial polymerization. Also, membrane partition coefficient of MPD shows the affinity of MPD to sublayer increase from 0.67 to 1.08 with increasing the ALD cycle of TiO_2 coating on the PES membrane (Table 1). In fact, the negatively charged TiO_2 layer leads to a strong electrostatic attraction between MPD and PES-TiO_2 layer because MPD is positively charged [64]. Also, PES-TiO_2 sublayer includes considerable amount of functional groups (hydroxyl) interacting with amine monomers via hydrogen bonds and covalent bonds [16,22,31]. Thus, there is a high affinity between MPD and PES-TiO_2, which is consistent with membrane partition coefficient of MPD results.

3.2. The properties of PA-TFC-x

After interfacial polymerization, the obtained PA-TFC-x membranes were imaged by FE-SEM. The selective PA layer was found to be full of folded nodular structures and randomly distributed protuberances on the uncoated PES sublayer (Fig. 3A). On the contrary, the surfaces of PA-TFC-x membranes become smoother and smoother with the increased number of ALD cycles as displayed in Fig. 3 (B-E). Moreover, the population and size of nodules also decrease with the increase of the ALD cycles of the TiO_2 on the PES support layer. Similar to the surface SEM images, AFM images of the surfaces of PA-TFC-x membranes in Fig. 3 (F-J) also show the decreasing trend in surface roughness. According to Fig. 4A, the polyamide layer on the coated sublayer (PA-TFC-200) has the smoothest surface, exhibiting the Ra value of 54 ± 4.32 nm, 35% lower than that of PA layer on uncoated PES membrane (81.76 ± 14.74 nm). The change in the roughness of PA layers lies mainly in the alteration of wettability and roughness of the underlying support membrane. The aqueous solution of MPD cannot homogenously cover the uncoated PES layer due to the low wettability of the surface and the non-uniform diffusion of MPD during IP process, resulting in rough PA layer. As the roughness and surface wettability of ALD-x-TiO_2@PES decreases and increases, respectively, the PA layers turn into smooth, which is in agreement with the literature [29,50,53].

The continuous polyamide films were clearly observed on top of the sublayers from the cross-sectional SEM images in Fig. 3 (L-P) and Fig. S3. By comparison of the thickness of the PA selective layer, shown in Fig. 4A and Table S2, it is obvious that the TiO_2 coating can lessen the thickness of the PA selective layer, changing from 216.2 ± 12.57 nm for PA on pristine PES membrane to 153.6 ± 9.6 nm for PA-TFC-200. The decreased thickness of the PA layer can be ascribed to two factors, which are also accord with the kinetic model [65,66] for thin film formation which was presented by Freger [67]. Firstly, the change of IP reaction leads to the different formation of the initial nuclei of the polyamide layers. The primarily formed polyamide layer will have a high degree of crosslinking if there is more amount of MPD in the reaction zone during IP, which were approved by the solution uptake test.

Table 1
Summary of properties related to affinity to amine solution for sublayers.

Sample	Membrane partition coefficient (K_m)	solution uptake (%)
PES	0.6731	3.114
ALD-10-TiO_2@PES	1.0321	4.162
ALD-50-TiO_2@PES	0.9552	4.238
ALD-100-TiO_2@PES	1.0616	4.516
ALD-200-TiO_2@PES	1.0848	4.781

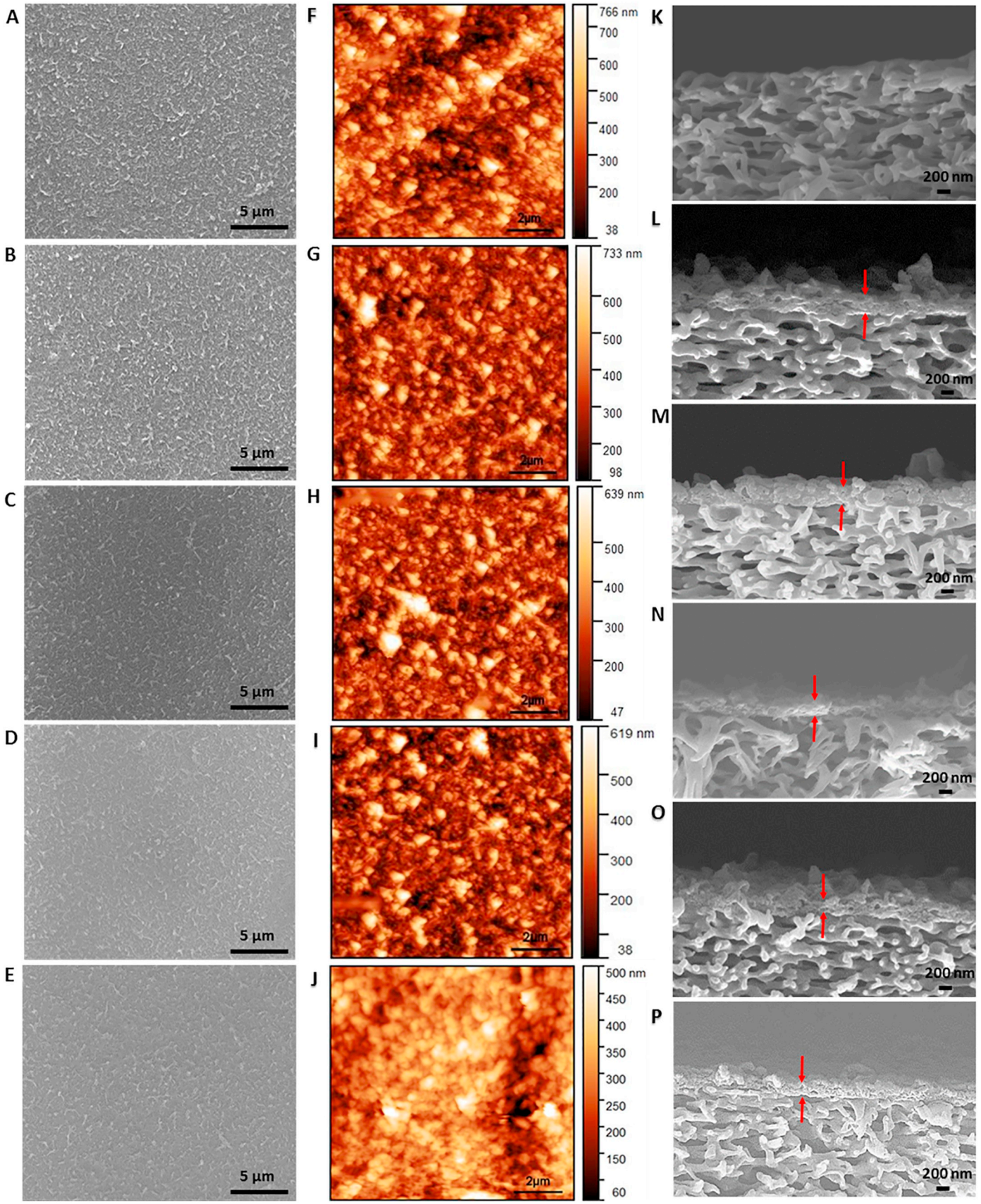

Fig. 3. SEM and AFM image of the TFC RO membranes (A, F) PA-TFC-0, (B, G) PA-TFC-10, (C, H) PA-TFC-50, (C, H) PA-TFC-100, (E, J) PA-TFC-200. (K to P) cross-sectional SEM images: (K) Pristine PES, (L) PA-TFC-0, (M) PA-TFC-10, (N) PA-TFC-50, (O) PA-TFC-100, and (P)PA-TFC-200.

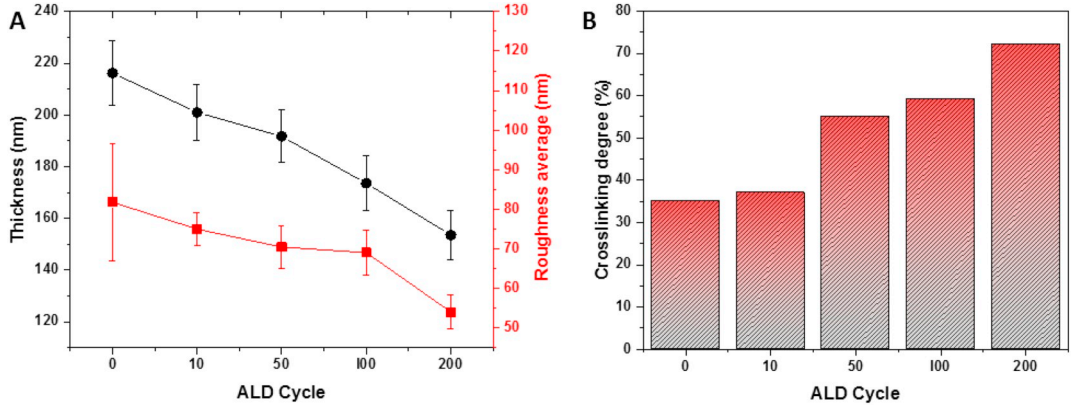

Fig. 4. Dependency of properties of Polyamide top selective layer of RO TFC membranes on PES/TiO2 sublayer with different ALD cycles (A) Graph showing (Ra) surface roughness and thickness (B) Crosslinking degree.

Then, the further diffusion of MPD will be hindered by the highly cross-linked polyamide film [29]. This nucleation could allow the thinner PA layer with smaller ridges and valleys to be fabricated. Secondly, after formation of the preliminary thin layer of polyamide, amine monomers are unceasingly released through the pores and partitioned into the organic phase [10,34]. The sublayer's affinity to MPD will affect the penetration of amine monomers through the preliminary layer. There is a high affinity between MPD and PES-TiO_2, which is consistent with membrane partition coefficient of MPD results, and contributes to a limited diffusion of amine monomers through the preliminary layer. Also, this confined and regulated amine diffusion would lead to the fabrication of the smoother and thinner selective PA layer [53].

The cross-linking degree and elemental composition of the polyamide active layer were assessed by XPS analysis. Spectra of XPS for TFC with different sublayers are shown in Fig. S2 and the consistent values of element composition, crosslinking degree are listed in Table S3. The XPS survey spectra of TFC membranes illustrate three major peaks of oxygen (O 1 s), carbon (C 1 s) and nitrogen (N 1 s) at the membrane surfaces as an indication of polyamide structure. The elemental composition results show that the O/N ratio of the polyamide layer declines with the increase of ALD cycle of TiO_2 on the PES support layer, indicating an increase of crosslinking degree. Based on the solution uptake test by increasing the ALD cycle of TiO_2 on the PES sublayer, the amount of amino monomer in the reaction zone increases which leads to the enhancement of polymerization efficiency and progress of the crosslinking degree of the polyamide layer that can be showed by Fig. 4B.

Therefore, presence of TiO_2 layer on the PES sublayer increase the amount of MPD in the concentration zone and limit the diffusion rate of the MPD molecules through the IP process. As a consequence, a thin and smooth polyamide skin layer with high cross-linking density and without defect fabricated at the interface.

3.3. Membrane transport properties

Fig. 5 depicts the performance of the PA-TFC-(0, 10, 50, 100, 200). The pure water permeation of the PA-TFC RO membrane rises from 1.4 to 1.8 $L.m^{-2}.h^{-1}.bar^{-1}$ for PA-TFC-0 to PA-TFC-100. This observation is expected because the membrane thickness, which is the main transmembrane resistance [68], decreases with the introduction of the TiO_2 layer as displayed in the FESEM images of the cross-section (Fig. 3 and Fig. S3). Also, the TiO_2 coating on the surface and pores of the support layer makes the water transport path faster and thus improves the water flux. It can also be seen that the NaCl rejection gradually rises at the same time from 92.6 to 96 with the increase of the ALD cycle of the TiO_2 on the PES support from 0 to 100. This increase in rejection is because of the increase in the crosslinking degree of the PA layer and formation of the uniform and defect-free PA layer on the sublayer. Once extended the ALD cycle of TiO_2 to 200, the TFC RO membranes demonstrated a decline in NaCl rejection (~88%). This trend can be attributed to the enhanced hydrophilicity of the sublayer. As revealed in Fig. 2I, when the ALD cycle is 200, the water contact angle declines below 20°. Therefore, instead of being reserved, the aqueous phase may penetrate through the sublayer which results in a discontinuous PA selective top layer. Accordingly, the salt rejection decreases, and the water permeation increases.

Totally, the ALD coating of TiO_2 has been shown to be an effective modification method to tune the sublayer properties and to make a favorable platform for the interfacial polymerization reaction of selective layers. The optimized ALD cycle of TiO_2, 100, leads to a PA-TFC RO membrane which had a superior performance (1.8 $L.m^{-2}.hr^{-1}.bar^{-1}$, 96.1%) compared to that of the PA-TFC membrane on the neat PES sublayer (1.4 $L.m^{-2}.h^{-1}.bar^{-1}$, 92.6%). Moreover, table S5 as a comparison between the PA-TFC-x membrane in this study and the commercial PA TFC membranes indicates that the TFC membrane with an interlayer of TiO_2 is within the range of or better than the performance of commercial membranes [69].

4. Conclusion

In this study, for the first time the low temperature ALD of TiO_2 as a functional nanomaterial was applied to tune the PES sublayer for developing the performance and properties of PA-TFC RO membranes via regulation of the adsorption/diffusion of amine monomer for the IP. The research results indicate that PES-TiO_2 platform leads to thin, smooth, no-defect and high cross-linked polyamide selective layer. On the other hand, it should consider a caution when the ALD technique is used because of the hydrophilicity of the coating layer, applying a large number of ALD cycles (200 cycle) will result in the discontinues polyamide layer and decline in the rejection, which is not appropriate in most applications. As a result, the TFC membranes on the sublayer with the optimum TiO_2 ALD coating (100 cycle) exhibited the superior performance for both water permeation and salt rejection. Therefore, ALD coating of TiO_2 as a functional nanomaterial on the sublayer may be a promising candidate to prepare high performance PA TFC membranes for desalination application to employed in industry.

CRediT authorship contribution statement

Kiyoumars Zarshenas:Conceptualization, Investigation, Methodology, Validation, Writing - original draft.**Gaopeng Jiang**:Methodology, Writing - review & editing.**Jing Zhang**:Writing - review & editing.**Mohd Altamash Jauhar**:Investigation.**Zhongwei Chen**:Supervision.

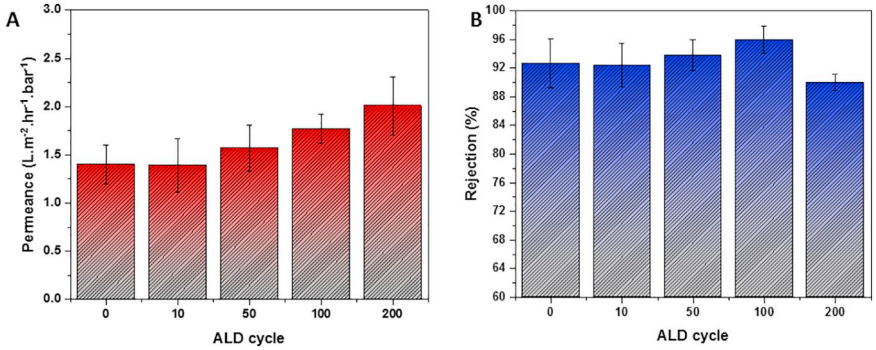

Fig. 5. Performance of PA-TFC-x RO membranes (A) Permeance (B) Rejection.

Acknowledgements

The authors acknowledge the financially support provided by the Natural Sciences and Engineering Research Council of Canada (NSERC), and Nanomaterials and Clean Energy Laboratory at the University of Waterloo.

Appendix A. Supplementary data

Supplementary data to this article can be found online at https://doi.org/10.1016/j.desal.2020.114342.

References

[1] M. Elimelech, W.A. Phillip, The future of seawater desalination: energy, technology, and the environment, Science (80-.) 333 (2011) 712–717, https://doi.org/10.1126/science.1200488.
[2] C.Y. Tang, Z. Yang, H. Guo, J.J. Wen, L.D. Nghiem, E. Cornelissen, Potable water reuse through advanced membrane technology, Environ. Sci. Technol. 52 (2018) 10215–10223, https://doi.org/10.1021/acs.est.8b00562.
[3] S.F. Anis, R. Hashaikeh, N. Hilal, Reverse osmosis pretreatment technologies and future trends: a comprehensive review, Desalination 452 (2019) 159–195, https://doi.org/10.1016/j.desal.2018.11.006.
[4] S. Jiang, Y. Li, B.P. Ladewig, A review of reverse osmosis membrane fouling and control strategies, Sci. Total Environ. 595 (2017) 567–583, https://doi.org/10.1016/j.scitotenv.2017.03.235.
[5] S.S. Shenvi, A.M. Isloor, A.F. Ismail, A review on RO membrane technology: developments and challenges, Desalination 368 (2015) 10–26, https://doi.org/10.1016/j.desal.2014.12.042.
[6] J.E. Cadotte, R.J. Petersen, R.E. Larson, E.E. Erickson, A new thin-film composite seawater reverse osmosis membrane, Desalination 32 (1980) 25–31, https://doi.org/10.1016/S0011-9164(00)86003-8.
[7] P.W. Morgan, S.L. Kwolek, Interfacial polycondensation. II. Fundamentals of polymer formation at liquid interfaces, J. Polym. Sci. Part A Polym. Chem. 34 (1996) 531–559, https://doi.org/10.1002/pola.1996.816.
[8] G.R. Xu, J.M. Xu, H.J. Feng, H.L. Zhao, S.B. Wu, Tailoring structures and performance of polyamide thin film composite (PA-TFC) desalination membranes via sublayers adjustment-a review, Desalination 417 (2017) 19–35, https://doi.org/10.1016/j.desal.2017.05.011.
[9] A.F. Ismail, M. Padaki, N. Hilal, T. Matsuura, W.J. Lau, Thin film composite membrane — recent development and future potential, Desalination 356 (2015) 140–148, https://doi.org/10.1016/j.desal.2014.10.042.
[10] A.K. Ghosh, E.M.V. Hoek, Impacts of support membrane structure and chemistry on polyamide-polysulfone interfacial composite membranes, J. Memb. Sci. 336 (2009) 140–148, https://doi.org/10.1016/j.memsci.2009.03.024.
[11] M.F. Jimenez-Solomon, P. Gorgojo, M. Munoz-Ibanez, A.G. Livingston, Beneath the surface: influence of supports on thin film composite membranes by interfacial polymerization for organic solvent nanofiltration, J. Memb. Sci. 448 (2013) 102–113, https://doi.org/10.1016/j.memsci.2013.06.030.
[12] Q. Zhang, Z. Zhang, L. Dai, H. Wang, S. Li, S. Zhang, Novel insights into the interplay between support and active layer in the thin film composite polyamide membranes, J. Memb. Sci. 537 (2017) 372–383, https://doi.org/10.1016/j.memsci.2017.05.033.
[13] G.Z. Ramon, M.C.Y. Wong, E.M.V. Hoek, Transport through composite membrane, part 1: is there an optimal support membrane? J. Memb. Sci. 415–416 (2012) 298–305, https://doi.org/10.1016/j.memsci.2012.05.013.
[14] X. Lu, L.H. Arias Chavez, S. Romero-Vargas Castrillón, J. Ma, M. Elimelech, Influence of active layer and support layer surface structures on organic fouling propensity of thin-film composite forward osmosis membranes, Environ. Sci. Technol. 49 (2015) 1436–1444, https://doi.org/10.1021/es5044062.
[15] J. Wang, R. Xu, F. Yang, J. Kang, Y. Cao, M. Xiang, Probing influences of support layer on the morphology of polyamide selective layer of thin film composite membrane, J. Memb. Sci. 556 (2018) 374–383, https://doi.org/10.1016/j.memsci.2018.04.011.
[16] A. Sotto, A. Rashed, R.X. Zhang, A. Martínez, L. Braken, P. Luis, B. Van der Bruggen, Improved membrane structures for seawater desalination by studying the influence of sublayers, Desalination 287 (2012) 317–325, https://doi.org/10.1016/j.desal.2011.09.024.
[17] J. Lee, R. Wang, T.H. Bae, High-performance reverse osmosis membranes fabricated on highly porous microstructured supports, Desalination 436 (2018) 48–55, https://doi.org/10.1016/j.desal.2018.01.037.
[18] Y. Zhu, W. Xie, S. Gao, F. Zhang, W. Zhang, Z. Liu, J. Jin, Single-walled carbon nanotube film supported nanofiltration membrane with a nearly 10 nm thick polyamide selective layer for high-flux and high-rejection desalination, Small 12 (2016) 5034–5041, https://doi.org/10.1002/smll.201601253.
[19] X. Zhao, J. Li, C. Liu, A novel TFC-type FO membrane with inserted sublayer of carbon nanotube networks exhibiting the improved separation performance, Desalination 413 (2017) 176–183, https://doi.org/10.1016/j.desal.2017.03.021.
[20] S.F. Anis, R. Hashaikeh, N. Hilal, Functional materials in desalination: a review, Desalination 468 (2019) 114077, , https://doi.org/10.1016/j.desal.2019.114077.
[21] M. Shi, Z. Wang, S. Zhao, J. Wang, P. Zhang, X. Cao, A novel pathway for high performance RO membrane: preparing active layer with decreased thickness and enhanced compactness by incorporating tannic acid into the support, J. Memb. Sci. 555 (2018) 157–168, https://doi.org/10.1016/j.memsci.2018.03.025.
[22] D. Emadzadeh, W.J. Lau, T. Matsuura, M. Rahbari-Sisakht, A.F. Ismail, A novel thin film composite forward osmosis membrane prepared from PSf-TiO2 nanocomposite substrate for water desalination, Chem. Eng. J. 237 (2014) 70–80, https://doi.org/10.1016/j.cej.2013.09.081.
[23] Q. Shi, L. Ni, Y. Zhang, X. Feng, Q. Chang, J. Meng, Poly(p-phenylene terephthamide) embedded in a polysulfone as the substrate for improving compaction resistance and adhesion of a thin film composite polyamide membrane, J. Mater. Chem. A 5 (2017) 13610–13624, https://doi.org/10.1039/C7TA02552A.
[24] S. Gao, Y. Zhu, Y. Gong, Z. Wang, W. Fang, J. Jin, Ultrathin polyamide nanofiltration membrane fabricated on brush-painted single-walled carbon nanotube network support for ion sieving, ACS Nano 13 (2019) 5278–5290, https://doi.org/10.1021/acsnano.8b09761.
[25] J.-J. Wang, H.-C. Yang, M.-B. Wu, X. Zhang, Z.-K. Xu, Nanofiltration membranes with cellulose nanocrystals as an interlayer for unprecedented performance, J. Mater. Chem. A 5 (2017) 16289–16295, https://doi.org/10.1039/C7TA00501F.
[26] Z. Zhou, Y. Hu, C. Boo, Z. Liu, J. Li, L. Deng, X. An, High-performance thin-film composite membrane with an ultrathin spray-coated carbon nanotube interlayer, Environ. Sci. Technol. Lett. 5 (2018) 243–248, https://doi.org/10.1021/acs.estlett.8b00169.
[27] W. Zhao, H. Liu, Y. Liu, M. Jian, L. Gao, H. Wang, X. Zhang, Thin-film nanocomposite forward-osmosis membranes on hydrophilic microfiltration support with an intermediate layer of graphene oxide and multiwall carbon nanotube, ACS Appl. Mater. Interfaces 10 (2018) 34464–34474, https://doi.org/10.1021/acsami.8b10550.
[28] G. Gong, P. Wang, Z. Zhou, Y. Hu, New insights into the role of an interlayer for the fabrication of highly selective and permeable thin-film composite nanofiltration membrane, ACS Appl. Mater. Interfaces 11 (2019) 7349–7356, https://doi.org/10.1021/acsami.8b18719.
[29] X. Zhang, Y. Lv, H.-C. Yang, Y. Du, Z.-K. Xu, Polyphenol coating as an interlayer for thin-film composite membranes with enhanced nanofiltration performance, ACS Appl. Mater. Interfaces 8 (2016) 32512–32519, https://doi.org/10.1021/acsami.6b10693.
[30] L. Wang, M. Fang, J. Liu, J. He, J. Li, J. Lei, Layer-by-layer fabrication of high-performance polyamide/ZIF-8 nanocomposite membrane for nanofiltration applications, ACS Appl. Mater. Interfaces 7 (2015) 24082–24093, https://doi.org/10.1021/acsami.5b07128.
[31] X.W. Liu, Y. Cao, Y.X. Li, Z.L. Xu, Z. Li, M. Wang, X.H. Ma, High-performance polyamide/ceramic hollow fiber TFC membranes with TiO 2 interlayer for pervaporation dehydration of isopropanol solution, J. Memb. Sci. 576 (2019) 26–35, https://doi.org/10.1016/j.memsci.2019.01.023.
[32] M. Wu, J. Yuan, H. Wu, Y. Su, H. Yang, X. You, R. Zhang, X. He, N.A. Khan, R. Kasher, Z. Jiang, Ultrathin nanofiltration membrane with polydopamine-covalent organic framework interlayer for enhanced permeability and structural

stability, J. Memb. Sci. 576 (2019) 131–141, https://doi.org/10.1016/j.memsci.2019.01.040.
[33] H. Choi, A.A. Shah, S.-E. Nam, Y.-I. Park, H. Park, Thin-film composite membranes comprising ultrathin hydrophilic polydopamine interlayer with graphene oxide for forward osmosis, Desalination 449 (2019) 41–49, https://doi.org/10.1016/j.desal.2018.10.012.
[34] S. Karan, Z. Jiang, A.G. Livingston, Sub-10 nm polyamide nanofilms with ultrafast solvent transport for molecular separation, Science 348 (2015) 1347–1351, https://doi.org/10.1126/science.aaa5058 80-.
[35] Z. Wang, Z. Wang, S. Lin, H. Jin, S. Gao, Y. Zhu, J. Jin, Nanoparticle-templated nanofiltration membranes for ultrahigh performance desalination, Nat. Commun. 9 (2018) 2004, https://doi.org/10.1038/s41467-018-04467-3.
[36] N.P. Dasgupta, L. Li, X. Sun, Atomic layer deposition for energy and environmental applications, Adv. Mater. Interfaces 3 (2016) 2–3, https://doi.org/10.1002/admi.201600914.
[37] R.W. Johnson, A. Hultqvist, S.F. Bent, A brief review of atomic layer deposition : from fundamentals to applications, Biochem. Pharmacol. 17 (2014) 236–246, https://doi.org/10.1016/j.mattod.2014.04.026.
[38] M. Weber, A. Julbe, A. Ayral, P. Miele, M. Bechelany, Atomic layer deposition for membranes: basics, challenges, and opportunities, Chem. Mater. 30 (2018) 7368–7390, https://doi.org/10.1021/acs.chemmater.8b02687.
[39] H. Yang, R.Z. Waldman, Z. Chen, S.B. Darling, Atomic layer deposition for membrane interface engineering, Nanoscale 10 (2018) 20505–20513, https://doi.org/10.1039/C8NR08114J.
[40] J. Feng, S. Xiong, Z. Wang, Z. Cui, S. Sun, Y. Wang, Atomic layer deposition of metal oxides on carbon nanotube fabrics for robust, hydrophilic ultra fi ltration membranes, J. Memb. Sci. 550 (2018) 246–253, https://doi.org/10.1016/j.memsci.2018.01.003.
[41] F. Li, Y. Yang, Y. Fan, W. Xing, Y. Wang, Modification of ceramic membranes for pore structure tailoring : the atomic layer deposition route, J. Memb. Sci. 397–398 (2012) 17–23, https://doi.org/10.1016/j.memsci.2012.01.005.
[42] X. Zhou, Y. Zhao, S.-R. Kim, M. Elimelech, S. Hu, J. Kim, Controlled TiO 2 growth on reverse osmosis and nanofiltration membranes by atomic layer deposition: mechanisms and potential applications, Environ. Sci. Technol. 52 (2018) 14311–14320, https://doi.org/10.1021/acs.est.8b03967.
[43] P. Juholin, M. Kääriäinen, M. Riihimäki, R. Sliz, J.L. Aguirre, M. Pirilä, T. Fabritius, D. Cameron, R.L. Keiski, Comparison of ALD coated nanofiltration membranes to unmodified commercial membranes in mine wastewater treatment, Sep. Purif. Technol. 192 (2018) 69–77, https://doi.org/10.1016/j.seppur.2017.09.005.
[44] K. Kaliyappan, Z. Chen, Atomic-scale manipulation of electrode surface to construct extremely stable high-performance sodium ion capacitor, Nano Energy 48 (2018) 107–116, https://doi.org/10.1016/j.nanoen.2018.03.021.
[45] E. Bet-Moushoul, Y. Mansourpanah, K. Farhadi, M. Tabatabaei, TiO2 nanocomposite based polymeric membranes: a review on performance improvement for various applications in chemical engineering processes, Chem. Eng. J. 283 (2016) 29–46, https://doi.org/10.1016/j.cej.2015.06.124.
[46] J. Sekulić, J.E. ten Elshof, D.H.A. Blank, A microporous titania membrane for nanofiltration and pervaporation, Adv. Mater. 16 (2004) 1546–1550, https://doi.org/10.1002/adma.200306472.
[47] T. Tsuru, D. Hironaka, T. Yoshioka, M. Asaeda, Titania membranes for liquid phase separation: effect of surface charge on flux, Sep. Purif. Technol. 25 (2001) 307–314, https://doi.org/10.1016/S1383-5866(01)00057-0.
[48] Z. Song, M. Fathizadeh, Y. Huang, K.H. Chu, Y. Yoon, L. Wang, W.L. Xu, M. Yu, TiO2 nanofiltration membranes prepared by molecular layer deposition for water purification, J. Memb. Sci. 510 (2016) 72–78, https://doi.org/10.1016/j.memsci.2016.03.011.
[49] G. Lui, G. Li, X. Wang, G. Jiang, E. Lin, M. Fowler, A. Yu, Z. Chen, Flexible, three-dimensional ordered macroporous TiO 2 electrode with enhanced electrode–electrolyte interaction in high-power Li-ion batteries, Nano Energy 24 (2016) 72–77, https://doi.org/10.1016/j.nanoen.2016.03.019.
[50] J. Alam, M. Alhoshan, L.A. Dass, A.K. Shukla, M.R. Muthumareeswaran, M. Hussain, A.S. Aldwayyan, Atomic layer deposition of TiO2 film on a polyethersulfone membrane: separation applications, J. Polym. Res. 23 (2016) 183, https://doi.org/10.1007/s10965-016-1063-9.
[51] G.S. Lai, W.J. Lau, P.S. Goh, Y.H. Tan, B.C. Ng, A.F. Ismail, A novel interfacial polymerization approach towards synthesis of graphene oxide-incorporated thin film nanocomposite membrane with improved surface properties, Arab. J. Chem. 12 (2019) 75–87, https://doi.org/10.1016/j.arabjc.2017.12.009.
[52] L. Huang, J.R. McCutcheon, Impact of support layer pore size on performance of thin film composite membranes for forward osmosis, J. Memb. Sci. 483 (2015) 25–33, https://doi.org/10.1016/j.memsci.2015.01.025.
[53] X. Yang, Y. Du, X. Zhang, A. He, Z.K. Xu, Nanofiltration membrane with a mussel-inspired interlayer for improved permeation performance, Langmuir 33 (2017) 2318–2324, https://doi.org/10.1021/acs.langmuir.6b04465.
[54] W.H.J. Vaes, E.U. Ramos, H.J.M. Verhaar, C.J. Cramer, J.L.M. Hermens, Understanding and estimating membrane/water partition coefficients: approaches to derive quantitative structure property relationships, Chem. Res. Toxicol. 11 (1998) 847–854, https://doi.org/10.1021/tx970210y.
[55] Y. Jun, H. Zarrin, M. Fowler, Z. Chen, Functionalized titania nanotube composite membranes for high temperature proton exchange membrane fuel cells, Int. J. Hydrog. Energy 36 (2011) 6073–6081, https://doi.org/10.1016/j.ijhydene.2011.02.030.
[56] Z. Jiang, S. Karan, A.G. Livingston, Water transport through ultrathin polyamide nanofilms used for reverse osmosis, Adv. Mater. 30 (2018) 1705973, , https://doi.org/10.1002/adma.201705973.
[57] X. Liang, L.F. Hakim, G.D. Zhan, J.A. McCormick, S.M. George, A.W. Weimer, J.A. Spencer, K.J. Buechler, J. Blackson, C.J. Wood, J.R. Dorgan, Novel processing to produce polymer/ceramic nanocomposites by atomic layer deposition, J. Am. Ceram. Soc. 90 (2007) 57–63, https://doi.org/10.1111/j.1551-2916.2006.01359.x.
[58] X. Liang, D.M. King, P. Li, A.W. Weimer, Low-temperature atomic layer-deposited TiO 2 films with low photoactivity, J. Am. Ceram. Soc. 92 (2009) 649–654, https://doi.org/10.1111/j.1551-2916.2009.02940.x.
[59] H.C. Guo, E. Ye, Z. Li, M.Y. Han, X.J. Loh, Recent progress of atomic layer deposition on polymeric materials, Mater. Sci. Eng. C. 70 (2017) 1182–1191, https://doi.org/10.1016/j.msec.2016.01.093.
[60] A. Spende, N. Sobel, M. Lukas, R. Zierold, J.C. Riedl, L. Gura, I. Schubert, J.M.M. Moreno, K. Nielsch, B. Stühn, C. Hess, C. Trautmann, M.E. Toimil-Molares, TiO 2, SiO 2, and Al 2 O 3 coated nanopores and nanotubes produced by ALD in etched ion-track membranes for transport measurements, Nanotechnology 26 (2015) 335301, https://doi.org/10.1088/0957-4484/26/33/335301.
[61] A. Rahtu, M. Ritala, Reaction mechanism studies on the zirconium chloride-water atomic layer deposition process, J. Mater. Chem. 12 (2002) 1484–1489, https://doi.org/10.1039/b109846b.
[62] R. Hussin, K.L. Choy, X. Hou, Deposited Tio2 thin films by atomic layer deposition (ALD) for optical properties, ARPN J. Eng. Appl. Sci. 11 (2016) 7529–7533 http://www.arpnjournals.org/jeas/research_papers/rp_2016/jeas_0616_4470.pdf.
[63] J. Aarik, A. Aidla, T. Uustare, M. Ritala, M. Leskelä, Titanium isopropoxide as a precursor for atomic layer deposition: characterization of titanium dioxide growth process, Appl. Surf. Sci. 161 (2000) 385–395, https://doi.org/10.1016/S0169-4332(00)00274-9.
[64] P. Vouros, K. Biemann, The structural significance of doubly charged ion spectra. Phenylenediamine derivatives, Org. Mass Spectrom. 2 (1969) 375–386, https://doi.org/10.1002/oms.1210020406.
[65] A. Nowbahar, V. Mansard, J.M. Mecca, M. Paul, T. Arrowood, T.M. Squires, Measuring interfacial polymerization kinetics using microfluidic interferometry, J. Am. Chem. Soc. 140 (2018) 3173–3176, https://doi.org/10.1021/jacs.7b12121.
[66] V. Freger, Kinetics of film formation by interfacial Polycondensation, Langmuir 21 (2005) 1884–1894, https://doi.org/10.1021/la048085v.
[67] V. Freger, Nanoscale heterogeneity of polyamide membranes formed by interfacial polymerization, Langmuir 19 (2003) 4791–4797, https://doi.org/10.1021/la020920q.
[68] Z.X. Low, Y.T. Chua, B.M. Ray, D. Mattia, I.S. Metcalfe, D.A. Patterson, Perspective on 3D printing of separation membranes and comparison to related unconventional fabrication techniques, J. Memb. Sci. 523 (2017) 596–613, https://doi.org/10.1016/j.memsci.2016.10.006.
[69] B.-H. Jeong, E.M.V. Hoek, Y. Yan, A. Subramani, X. Huang, G. Hurwitz, A.K. Ghosh, A. Jawor, Interfacial polymerization of thin film nanocomposites: a new concept for reverse osmosis membranes, J. Memb. Sci. 294 (2007) 1–7, https://doi.org/10.1016/j.memsci.2007.02.025.